Proceedings of the 11th Brazilian Congress of Thermal Sciences and Engineering -- ENCIT 2006
Braz. Soc. of Mechanical Sciences and Engineering -- ABCM, Curitiba, Brazil, Dec. 5-8, 2006

Paper CIT06-0985

A NUMERICAL STUDY ON A CYLINDRICAL NON-TAPERED AXIALLY ROTATING HEAT PIPE WITH POROUS MEDIUM IN TERMS OF ITS OPERATIONAL LIMITS

Luís Edson Saraiva
Universidade de Passo Fundo – Faculdade de Engenharia e Arquitetura – Campus I – Bairro São José – Caixa Postal 611/631 – Passo Fundo – RS – 99001-970
saraiva@upf.br

Kamal Abdel Radi Ismail
Universidade Estadual de Campinas – Faculdade de Engenharia Mecânica - Cidade Universitária Zeferino Vaz- Rua Mendeleiev, 20 – Caixa Postal 6122 – Campinas – SP - 13083-860
kamal@fem.unicamp.br

Abstract. *This paper treats a two-dimensional model for the heat pipe rotating about its own axis. The heat pipe is internally and externally cylindrical with constant diameter and porous wick. The model is based upon the conservation equation of mass, momentum and energy. The vapor and liquid regions are solved as a coupled problem by the finite volume control method and the SIMPLE algorithm. Numerical simulations were performed varying the rotational speed and the heat transfer rate at the evaporator side. The results were plotted in terms of dimensionless parameters related to the operational limits of the heat pipe, to help design and dimensioning of heat pipes.*

Keywords: rotating heat pipe, porous wick, operation limits.

1. Introduction

Heat pipes are thermal equipments designed to transfer high heat fluxes over long distances with small temperature drop and without any external pumping work. This is achieved by using the latent heat of phase change of a suitable working fluid.

One type of heat pipe is called rotating heat pipe where the heat pipe rotates around its own axis, (Gray, 1969). Externally cylindrical rotating heat pipes are used in applications such as cooling of electric motors and generators, bearings and many other rotating machine elements. Disc type rotating heat pipes are used for cooling turbines and breaking drums.

Rotating heat pipes with conical internal geometry generate an axial component of the centrifugal force, which impels the fluid to return to the evaporator. Details of such systems can be found in references as (Daniels and Al-Jumaily, 1975; Daniels and Al-Baharnah, 1978; Daniels and Williams, 1978 and 1979; Li *et al.*, 1993; Ponnappan and He, 1998).

A rotating cylindrical heat pipe with a porous wick was studied by Miranda (1989) and Ismail and Miranda (1997). Their model is based upon the conservation equations of mass, momentum and energy for the liquid and vapor regions. These equations were solved by the finite difference technique and the finite volume method by using the SIMPLE algorithm. It was found that the increase of rotational speed beyond a certain critical value led to reversing the flow in the vapor region. This was found to occupy more and more of the vapor region with the increase of the rotational speed. These findings were later confirmed by Faghri *et al.* (1993) where they solved only the vapor region and Harley and Faghri (1995) where they solved numerically the flow problem in the liquid and vapor regions.

The present paper presents the results of a numerical simulation realized on a rotating heat pipe of internal and external constant diameter cylindrical geometry with a porous wick. The simulation of the rotating heat pipe is based upon the numerical solution of the conservation equations of mass, momentum and energy in the liquid and vapor regions. The results are presented in terms of dimensionless parameters in order to generalize the results and turn them useful for sizing and design of rotating heat pipe. Additional results can be found in Saraiva (2004).

2. Formulation of the problem

Figure (1) shows the physical model of the rotating heat pipe under study, where the heat flux $\dot{q}$ is applied to the evaporator and a similar heat flux $-\dot{q}$ is removed at the condenser. The vapor and liquid mass fluxes are $\dot{m}_v$ and $\dot{m}_l$, respectively.

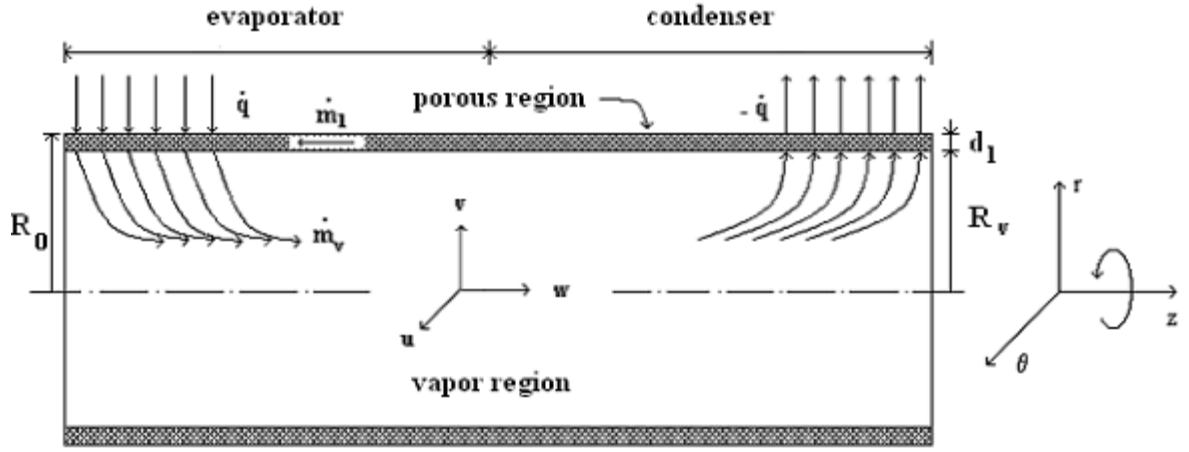

Figure 1 Scheme of the rotating heat pipe.

Adopting the coordinate system shown in Fig. (1), assuming two dimensional, axially symmetrical permanent incompressible flow in the liquid region and compressible in the vapor region, it is possible to write the conservation equations as

2.1. Vapor region

2.1.1. Conservation of mass

$$\frac{1}{r}\frac{\partial}{\partial r}\left(r\rho_v v_v\right)+\frac{\partial\left(\rho_v w_v\right)}{\partial z}=0 \tag{1}$$

2.1.2. Conservation of the momentum in the r, θ and z directions, respectively

$$\rho_v\left(v_v\frac{\partial v_v}{\partial r}-\frac{u_v^2}{r}+w_v\frac{\partial v_v}{\partial z}\right)=-\frac{\partial p_v}{\partial r}+\mu_v\left(\frac{\partial}{\partial \mathrm{r}}\left(\frac{1}{r}\frac{\partial}{\partial r}\left(rv_v\right)\right)+\frac{\partial^2 v_v}{\partial z^2}\right)$$
$$+\frac{1}{3}\mu_v\left(\frac{\partial}{\partial r}\left(\frac{1}{r}\frac{\partial\left(rv_v\right)}{\partial r}\right)+\frac{\partial^2 w_v}{\partial z\partial r}\right)+2\rho_v\Omega u_v+\rho_v\Omega^2 r \tag{2}$$

where Ω is the rotational speed.

$$\rho_v\left(v_v\frac{\partial u_v}{\partial r}-\frac{v_v u_v}{r}+w_v\frac{\partial u_v}{\partial z}\right)=\mu_v\left(\frac{\partial}{\partial r}\left(\frac{1}{r}\frac{\partial}{\partial r}\left(ru_v\right)\right)+\frac{\partial^2 u_v}{\partial z^2}\right)-2\rho_v\Omega v_v \tag{3}$$

$$\rho_v\left(v_v\frac{\partial w_v}{\partial r}+w_v\frac{\partial w_v}{\partial z}\right)=-\frac{\partial p_v}{\partial z}+\mu_v\left(\frac{1}{r}\frac{\partial}{\partial r}\left(r\frac{\partial w_v}{\partial r}\right)+\frac{\partial^2 w_v}{\partial z^2}\right)+\frac{1}{3}\mu_v\left(\frac{\partial^2 w_v}{\partial z^2}+\frac{1}{r}\frac{\partial v_v}{\partial z}+\frac{\partial^2 v_v}{\partial z\partial r}\right) \tag{4}$$

2.1.3. Conservation of energy

$$\rho_v c_{p_v}\left(v_v\frac{\partial T_v}{\partial r}+w_v\frac{\partial T_v}{\partial z}\right)=k_v\left(\frac{1}{r}\frac{\partial}{\partial r}\left(r\frac{\partial T_v}{\partial r}\right)+\frac{\partial^2 T_v}{\partial z^2}\right)+v_v\frac{\partial p_v}{\partial r}+u_v\frac{\partial p_v}{\partial z}+\mu\Phi \tag{5}$$

where the viscous dissipation term Φ is written as

$$\Phi=2\left[\left(\frac{\partial v_v}{\partial r}\right)^2+\left(\frac{v_v}{r}\right)^2+\left(\frac{\partial w_v}{\partial z}\right)^2\right]+\left(\frac{\partial u_v}{\partial r}-\frac{u_v}{r}\right)^2+\left(\frac{\partial u_v}{\partial z}\right)^2+\left(\frac{\partial v_v}{\partial z}+\frac{\partial w_v}{\partial r}\right)^2-\frac{2}{3}\left(\frac{\partial v_v}{\partial r}+\frac{v_v}{r}+\frac{\partial w_v}{\partial z}\right)^2 \tag{6}$$

2.2. Liquid region

2.2.1. Conservation of mass

$$\frac{1}{r}\frac{\partial}{\partial r}\left(rv_l\right)+\frac{\partial w_l}{\partial z}=0 \tag{7}$$

2.2.2. Conservation of the momentum in the r, θ and z directions, respectively

$$\rho_l\left(v_l\frac{\partial v_l}{\partial r}-\frac{u_l^2}{r}+w_l\frac{\partial v_l}{\partial z}\right)=-\varepsilon\frac{\partial p_l}{\partial r}+\mu_l\left(\frac{\partial}{\partial r}\left(\frac{1}{r}\frac{\partial}{\partial r}\left(rv_l\right)\right)+\frac{\partial^2 v_l}{\partial z^2}\right)-\frac{\mu_l\varepsilon}{K}v_l+2\rho_l\Omega u_l+\rho_l\Omega^2 r \tag{8}$$

$$\rho_l\left(v_l\frac{\partial u_l}{\partial r}-\frac{v_l u_l}{r}+w_l\frac{\partial u_l}{\partial z}\right)=\mu_l\left(\frac{\partial}{\partial r}\left(\frac{1}{r}\frac{\partial}{\partial r}\left(ru_l\right)\right)+\frac{\partial^2 u_l}{\partial z^2}\right)-\frac{\mu_l\varepsilon}{K}u_l-2\rho_l\Omega v_l \tag{9}$$

$$\rho_l\left(v_l\frac{\partial w_l}{\partial r}+w_l\frac{\partial w_l}{\partial z}\right)=-\varepsilon\frac{\partial p_l}{\partial z}+\mu_l\left(\frac{1}{r}\frac{\partial}{\partial r}\left(r\frac{\partial w_l}{\partial r}\right)+\frac{\partial^2 w_l}{\partial z^2}\right)-\frac{\mu_l\varepsilon}{K}w_l \tag{10}$$

where ε is the porosity of the porous region and K is its permeability.

2.2.3. Conservation of energy

$$\rho_l c_{pl}\left(v_l\frac{\partial T_l}{\partial r}+w_l\frac{\partial T_l}{\partial z}\right)=\frac{k_{eff}}{\varepsilon}\left(\frac{1}{r}\frac{\partial}{\partial r}\left(r\frac{\partial T_l}{\partial r}\right)+\frac{\partial^2 T_l}{\partial z^2}\right)+v_l\frac{\partial p_l}{\partial r}+u_v\frac{\partial p_l}{\partial z}+\mu_l\Phi \tag{11}$$

where k_{eff} is the effective thermal conductivity of the porous medium and Φ is the viscous dissipation term.

$$\Phi=2\left[\left(\frac{\partial v_l}{\partial r}\right)^2+\left(\frac{v_l}{r}\right)^2+\left(\frac{\partial w_l}{\partial z}\right)^2-\frac{2}{3}\left(\frac{\partial v_l}{\partial r}+\frac{v_l}{r}+\frac{\partial w_l}{\partial z}\right)^2\right]+\left(\frac{\partial u_l}{\partial r}-\frac{u_l}{r}\right)^2+\left(\frac{\partial u_l}{\partial z}\right)^2+\left(\frac{\partial v_l}{\partial z}+\frac{\partial w_l}{\partial r}\right)^2 \tag{12}$$

The coupling between the momentum and energy equations is realized by using the state equation.

2.3. Boundary conditions

The pipe extremities are assumed adiabatic in relation to the energy equation and are ruled by the no-slip boundary condition for the momentum equation. Hence, at $z=0, L$:

$$\frac{\partial T_{v,l}}{\partial z}=0 \tag{13}$$

$$u_{v,l}=v_{v,l}=w_{v,l}=0 \tag{14}$$

Along the pipe axis of symmetry, $r=0$, the radial and tangential velocity components are zero and the radial gradient of axial velocity and temperature are also assumed zero, due to the symmetry condition:

$$u_v=v_v=0 \tag{15}$$

$$\frac{\partial w_v}{\partial r}=0 \tag{16}$$

$$\frac{\partial T_v}{\partial r}=0 \tag{17}$$

To couple the vapor and the liquid regions one assumes that phase change occurs on the porous surface, at the liquid-vapor interface. Hence, the liquid radial velocity at the liquid-vapor interface, $r = R_v$, is

$$v_l(z) = \frac{\dot{q}''(z) + k_v \left.\frac{\partial T_v}{\partial r}\right|_{r = R_v}}{\rho_l \lambda} \tag{18}$$

where $\dot{q}''(z)$ is the density of the local heat flux at the interface.

From the mass conservation at the interface, $r = R_v$, one can write

$$v_v(z) = \frac{\rho_l v_l(z)}{\rho_v} \varepsilon \tag{19}$$

Along the liquid-vapor interface, $r = R_v$, the tangential and axial velocities components are zero:

$$u_{v,l} = w_{v,l} = 0 \tag{20}$$

Because of the assumption of phase change at the interface, $r = R_v$, the vapor and liquid temperatures are equal:

$$T_l = T_v \tag{21}$$

On the external surface of the pipe, $r = R_0$, boundary conditions of the second type are assumed along the evaporator and condenser regions, respectively, with the non-slip condition,

$$k_{eff} \frac{\partial T_l}{\partial r} = \dot{q}'' \tag{22}$$

$$-k_{eff} \frac{\partial T_l}{\partial r} = \dot{q}'' \tag{23}$$

$$u_l = v_l = w_l = 0 \tag{24}$$

The equations of mass conservation, momentum and energy are solved simultaneously for the vapor and liquid regions using the finite control volume method and the algorithm SIMPLE (Patankar, 1980).

Numerical tests were realized to turn the numerical calculations independent of the grid size. For the present work, 60 control volumes along the axial direction and 17 control volumes along the radial direction in the vapor region, together with a grid of 60×5 control volumes along the axial and radial directions in the porous region are found to be adequate.

The present numerical model, the procedures and results are compared with the results due to Faghri *et al.* (1993) and the agreement is found to be good (Saraiva and Ismail, 2006). Similar comparative results were omitted for the sake of brevity.

3. Results and discussion

The rotating heat pipe used for the present study is of total length of 1.0 m where the evaporator and condenser are 0.5 m each with no adiabatic section. The porous wick thickness is 0.0073 m of sintered bronze particles of 0.000683 m mean radius. The internal radius of the tube is 0.0127 m and the porosity of the wick is 0.44.

Extensive numerical simulations were realized to permit the local analysis of the heat pipe under different operation conditions such as rotational speed and heat flux at the evaporator side. The results are presented in terms of the angular Reynolds number, related to the rotational velocity, and in terms of injection Reynolds number, related to the heat flux, defined successively as

Angular Reynolds number:

$$\mathrm{Re}_{ang} = \frac{\rho_v (\Omega R_v) 2R_v}{\mu_v} \tag{25}$$

Injection Reynolds number:

$$\mathrm{Re}_{inj} = \frac{\rho_v V_{inj} 2R_v}{\mu_v} \tag{26}$$

where the injection velocity is given by

$$V_{inj} = \frac{\dot{q}''}{\rho_v \lambda} \tag{27}$$

A tentative analysis to relate the operational limits of heat pipes to the non-dimensional parameters mentioned is tried. The analysis is done in terms of the capillary, the sonic, the entrainment and the boiling limits of a heat pipe as in Chi (1976) for conventional heat pipes.

The exceeding capillary pressure is defined as the difference between the maximum capillary pressure developed and the minimum local difference between the liquid and vapor pressures at the interface and can be written as

$$p_{ex} = \frac{2\sigma}{r_c} - \left[p_v(z) - p_l(z)\right]_{\min} \tag{28}$$

or in dimensionless form as

$$p'_{ex} = 1 - \frac{\left[p_v(z) - p_l(z)\right]_{\min}}{\frac{2\sigma}{r_c}} \tag{29}$$

Using the dimensionless variables and numbers presented above, sets of graphs for both, water and methanol, as working fluids are presented and discussed. Figure (2) shows the variation of the dimensionless exceeding capillary pressure in terms of the rotational Reynolds number. As can be seen, the limit ($p'_{ex} = 0$) is reached for very high rotational speeds (Re_{ang}) and is weakly dependent upon the heat transfer rate (Re_{inj}).

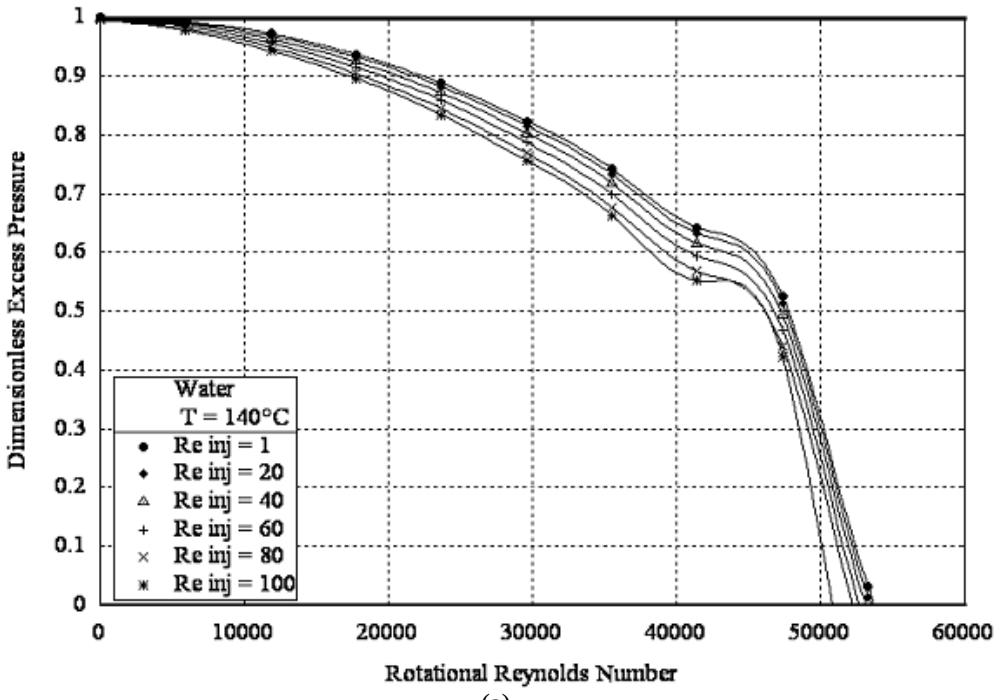

(a)

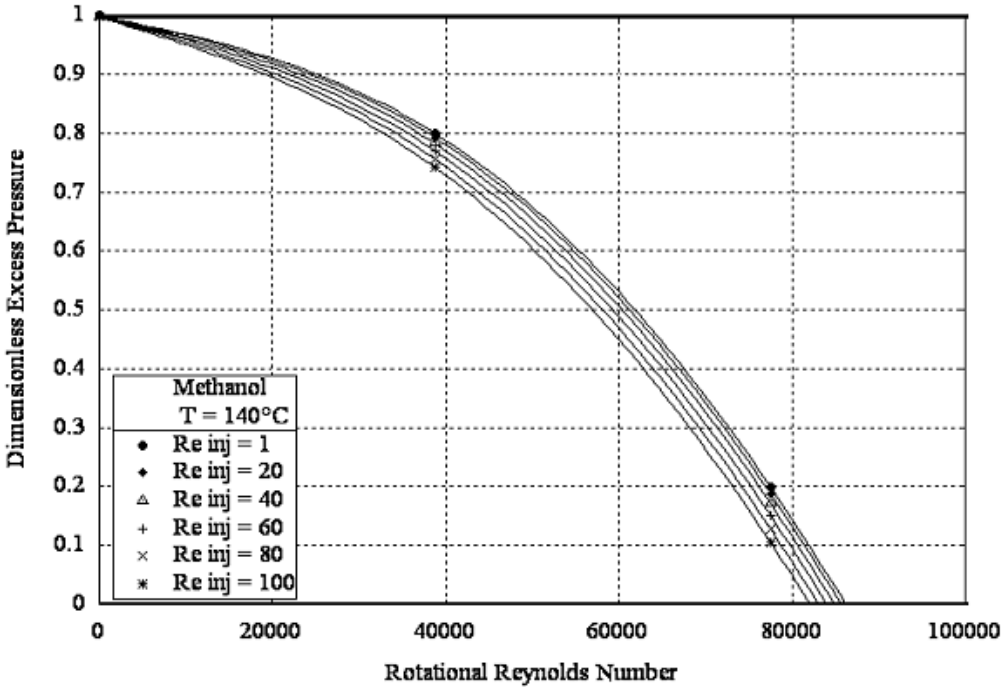

(b)

Figure 2 Dimensionless exceeding capillary pressure on the liquid-vapor interface, as a function of the angular Reynolds number, for some injection Reynolds numbers, for (a) water and (b) methanol.

In the present analysis the Mach number is defined in relation to the maximum axial velocity as

$$Ma_{ax} = \frac{w_{v\max}}{c} \tag{30}$$

and also in relation to the maximum tangential velocity as

$$Ma_{tg} = \frac{u_{v\max}}{c} \tag{31}$$

where the local sound velocity is given by

$$c = \sqrt{k_s R_g T} \tag{32}$$

Figures (3) and (4) indicate that the Mach numbers for axial and tangential flows are much lower than the sonic limit ($Ma = 1$) and that the Mach numbers are proportional to the heat transfer rate and the rotational speeds.

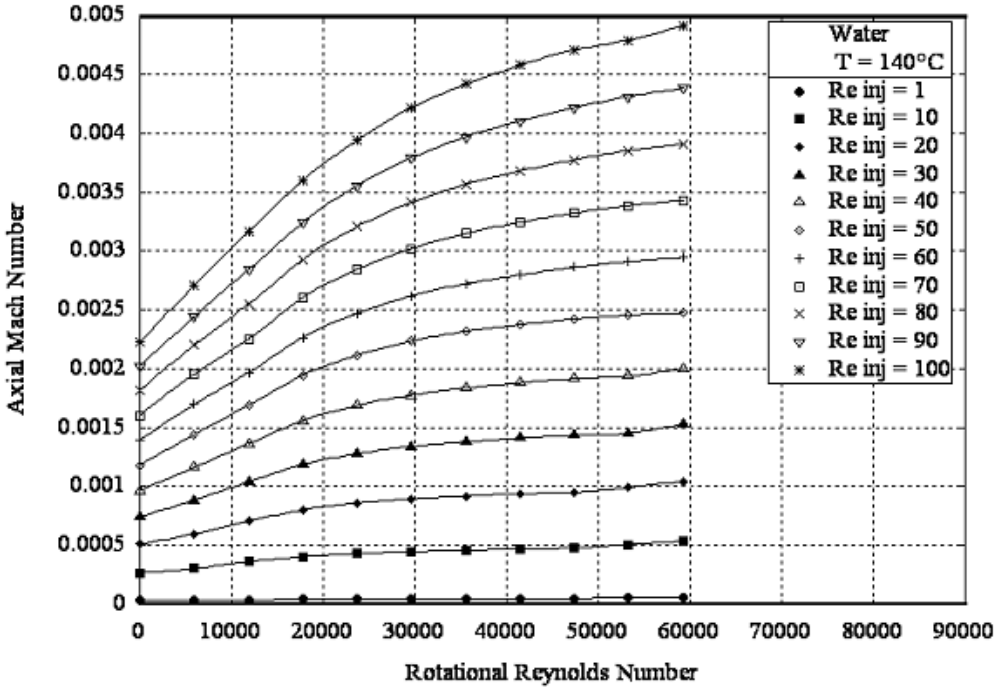

(a)

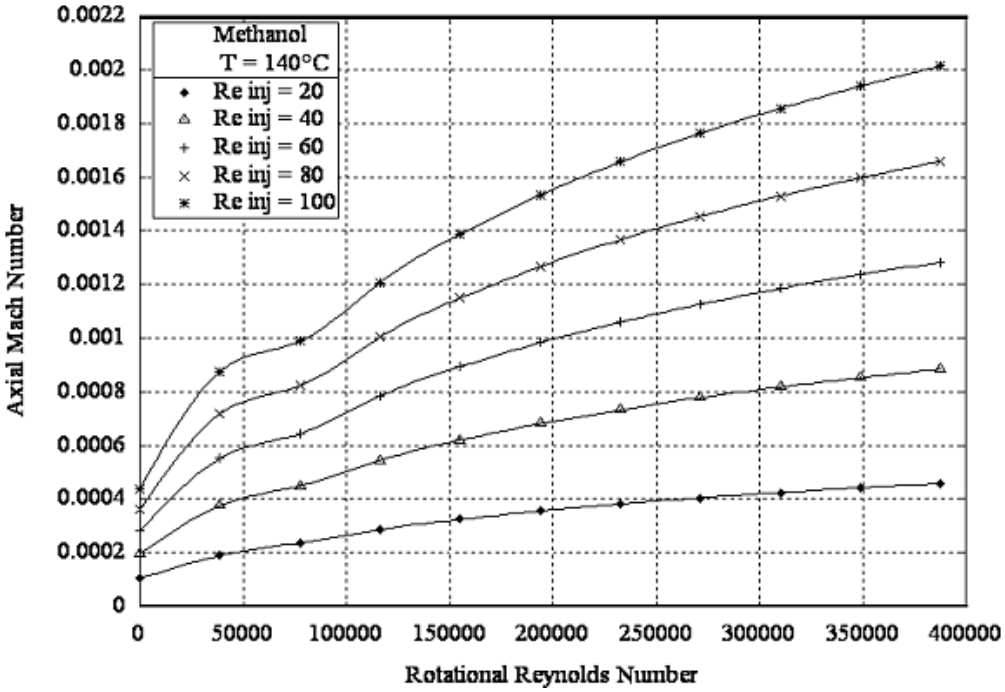

(b)

Figure 3. Mach number obtained in terms of maximum axial velocity of the vapor, at the evaporator, as a function of the angular Reynolds number, for some injection Reynolds numbers, for (a) water and (b) methanol.

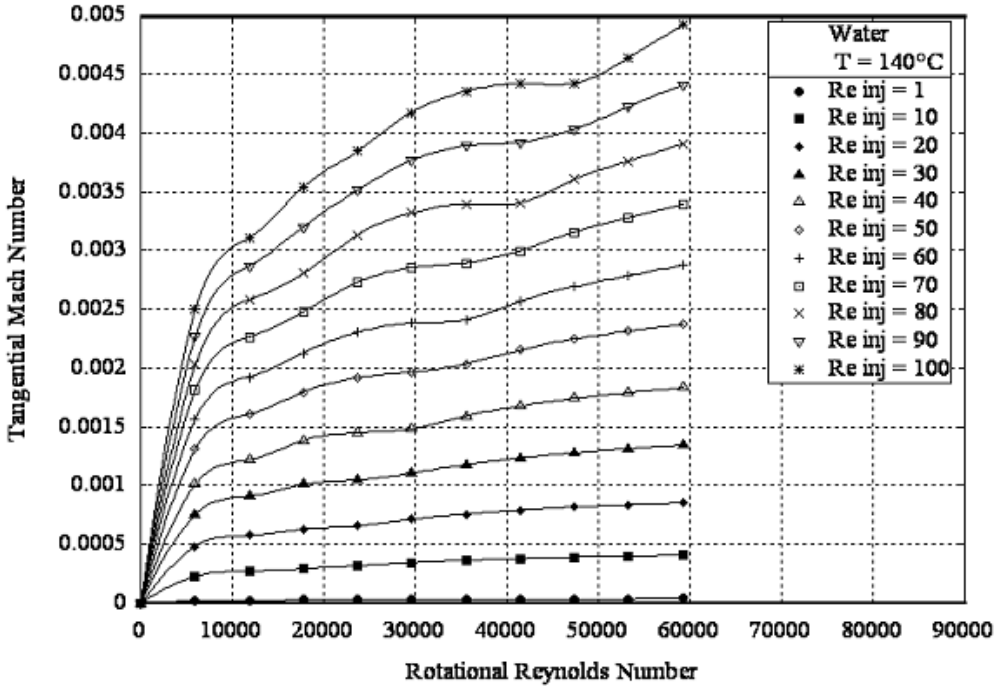

(a)

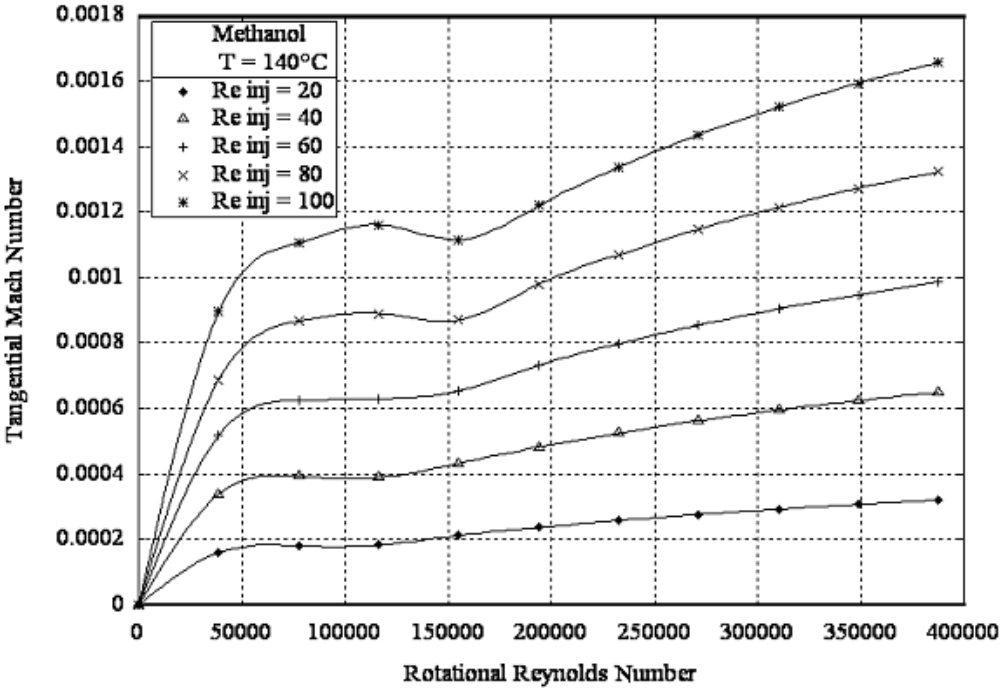

(b)

Figure 4. Mach number obtained in terms of maximum tangential velocity of the vapor, at the evaporator, as a function of the angular Reynolds number, for some injection Reynolds numbers, for (a) water and (b) methanol.

The entrainment limit is relate to the Weber number which is defined in relation to the maximum axial velocity component in the vapor, as

$$We_{ax} = \frac{\rho_v w_{v\,\max}^{\,2}\, 2r_c}{\sigma} \tag{33}$$

and in terms of the maximum tangential velocity in the vapor, as

$$We_{tg} = \frac{\rho_v u_v^{2}{}_{\max} 2r_c}{\sigma} \tag{34}$$

Figures (5) and (6) show the increase of Weber number with the increase of heat transfer rate and also with the increase of the rotational speed. Also one can observe that the Weber number is more sensitive to rotational speed when the heat transfer is high. It is worth mentioning here that the entrainment limit ($We = 1$) is too far to be reached.

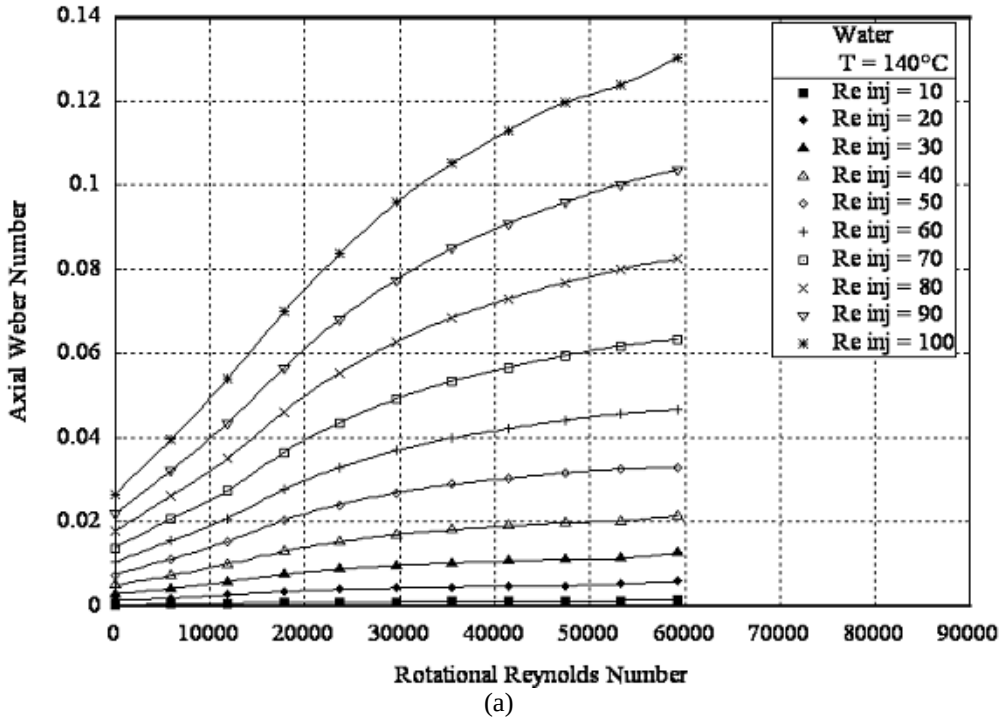

(a)

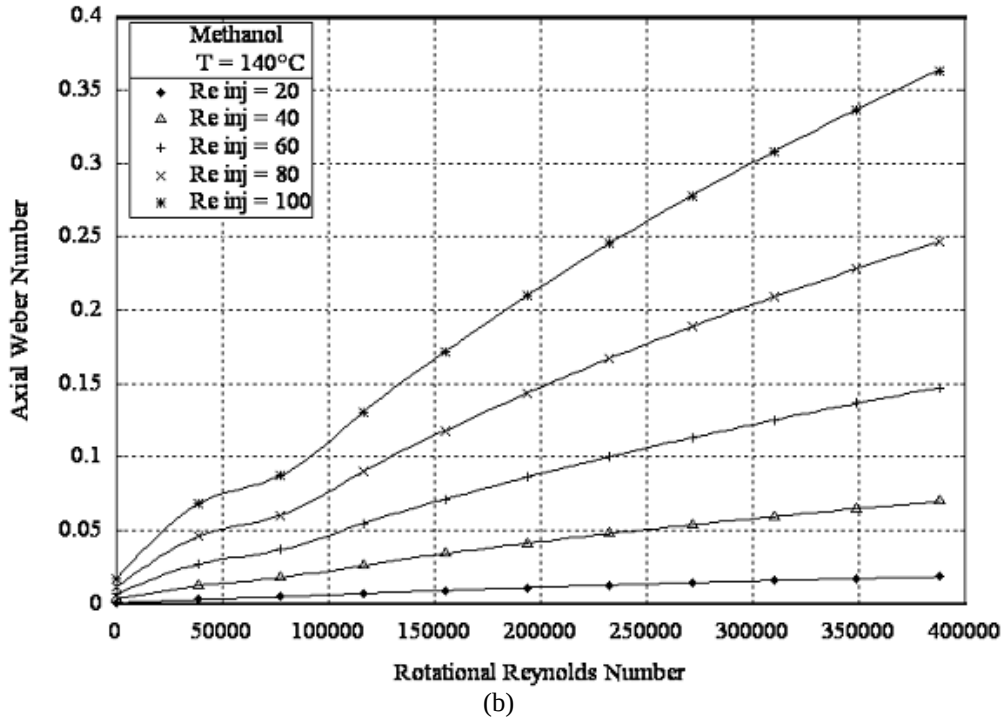

(b)

Figure 5. Weber number obtained in terms of maximum axial velocity of the vapor, at the evaporator, as a function of the angular Reynolds number, for some injection Reynolds numbers, for (a) water and (b) methanol.

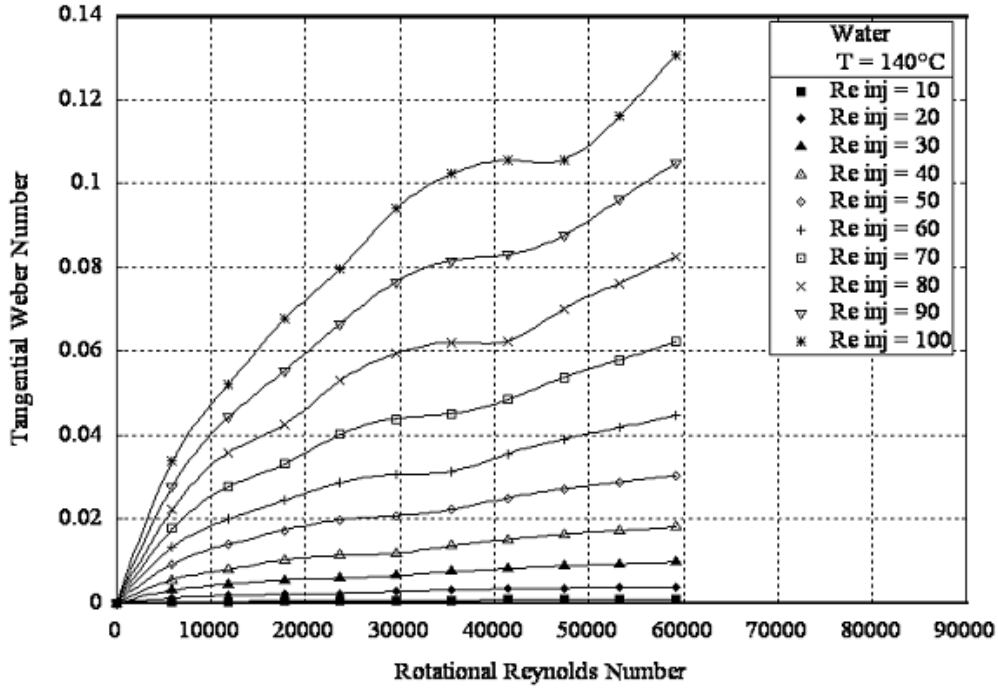

(a)

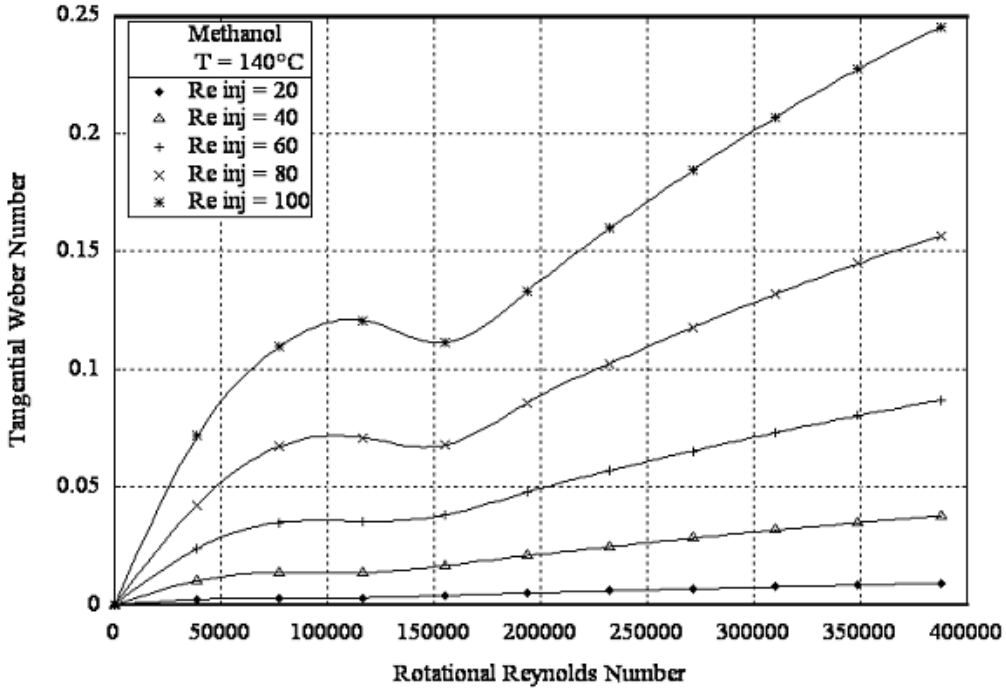

(b)

Figure 6. Weber number obtained in terms of maximum tangential velocity of the vapor, at the evaporator, as a function of the angular Reynolds number, for some injection Reynolds numbers, for (a) water and (b) methanol.

The maximum admissible heat transfer rate without vapor bubble formation in the porous wick is given by:

$$\dot{q}''_{\max} = \frac{k_{eff} T_v}{\lambda \rho_v R_0 \ln(R_0/R_v)} \left(2\sigma \left(\frac{1}{r_n} - \frac{1}{r_c} \right) \right) \tag{35}$$

Accordingly, dimensionless number related to the above taken as a limiting value for bubble formation in the porous medium is defined as

$$Bo = \frac{\dot{q}''\lambda\rho_v R_0 \ln\left(R_0/R_v\right)}{k_{eff} T_v \left(2\sigma\left(\frac{1}{r_n} - \frac{1}{r_c}\right)\right)} \tag{36}$$

where the initial radius of a vapor bubble in formation (r_n) adopted is equal to $2{,}5\times10^{-7}$ m.

Figure (7) shows the variation of the boiling dimensionless number in terms of the injection Reynolds number. A value of unity means that the boiling limit of the heat pipe has been achieved while a value between zero and unity results in safe operational conditions in relation to the impossibility of forming vapor bubbles.

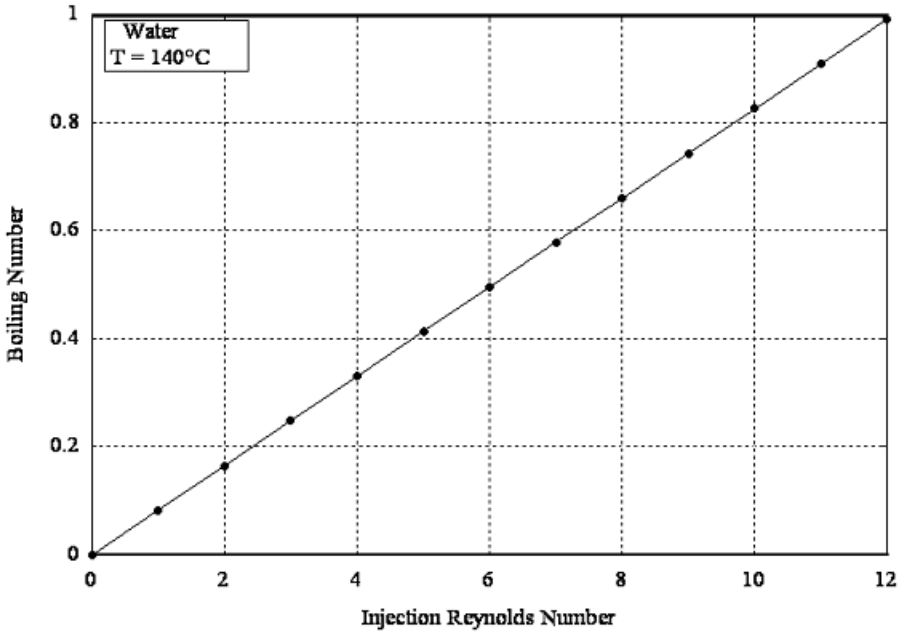

(a)

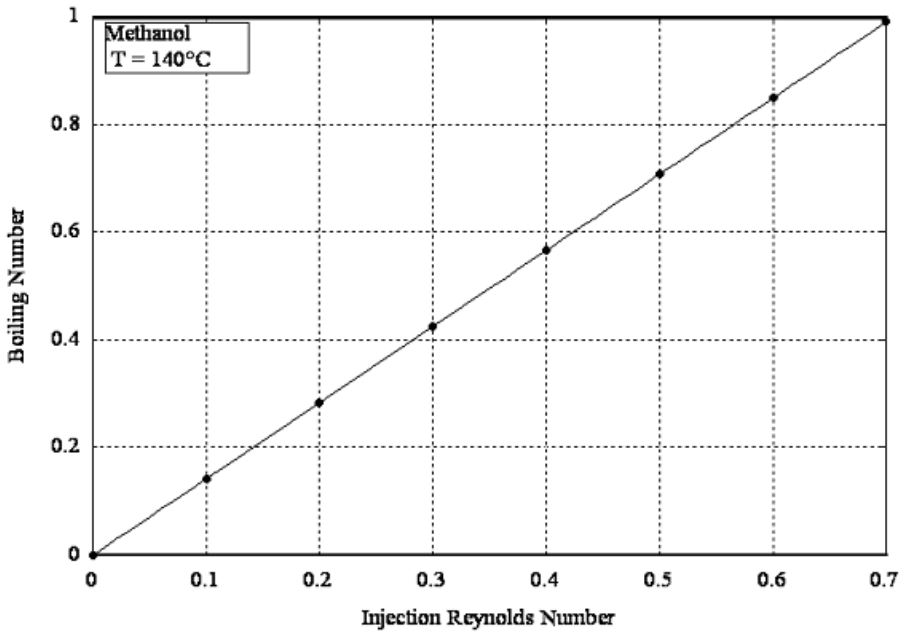

(b)

Figure 7. Boiling number, at the evaporator, as a function of the injection Reynold number, for (a) water and (b) methanol.

To demonstrate the utilization of these graphs to analyze the operational limits of rotating heat pipes, consider that it is required to transfer 10,000 W/m² at 3,600 rpm and it is required to investigate which of the two fluids, water or methanol, is most suitable for the application. From Figures (2) to (7) and by using Eqs. (25) to (27), it is possible to

construct Tab. 1. One can observe from Tab. 1 that water is the only suitable fluid to attend the established conditions. Methanol is shown to fail to attend the capillary and the boiling limits.

Table 1. Values of dimensionless numbers, calculated for a rotating heat pipe required to transport 10,000 W/m² at 3,600 rpm.

	p'_{ex}	Ma_{ax}	Ma_{tg}	We_{ax}	We_{tg}	Bo
Water Re_{inj} **= 8.8** Re_{ang} **= 17,756**	0.94	0.0003	0.00025	0.001	0.001	0.72
Methanol Re_{inj} **= 21.3** Re_{ang} **= 116,230**	Out of limit	0.0001	0.00007	0.005	0.003	Out of limit

4. Conclusions

This paper presents a two-dimensional model based upon the conservation equations of mass, momentum and energy, developed and solved numerically by using the finite volume control method and the SIMPLE algorithm. Simulations were performed and the results were plotted in terms of dimensionless numbers related to the operational limits of a rotating heat pipe, as an extension of the theory developed by Chi (1976). The graphs obtained were used to calculate a simple test case. These curves set up for different working fluids, boundary conditions and geometrical constraints should be useful for heat pipe analysis.

As shown, in order to obtain the operational limits of a particular heat pipe, a solution for the conservation equations must be achieved. In fact, due to the strong connection between operational limits and the very solution of the conservation equations, mainly in terms of velocities, it can be concluded that the quality of the results depends on the attachment between the mathematical model adopted and the physics of the problem. So, unfortunately, a simple methodology as proposed by Chi (1976) for conventional heat pipes, based upon an one-dimensional formulation, is likely inadequate to the complex behavior of a rotating heat pipe.

5. References

Chi, S.W., 1976, "Heat Pipe Theory and Practice: A Sourcebook", Hemisphere Publishing Corporation; McGraw-Hill Book Company, U.S.A., 242 p.

Daniels, T.C. and Al-Baharnah, N.S., 1978, "Temperature and Heat Load Distribution in Rotating Heat Pipes", Proceedings of the International Heat Pipe Conference, 3, pp.170-176.

Daniels, T.C. and Williams, R.J., 1978, "Experimental Temperature Distribution and Heat Load Characteristics of Rotating Heat Pipes", International Journal of Heat and Mass Transfer, Vol. 2, 193-201.

Daniels, T.C. and Williams, R.J., 1979, "The Effect of External Boundary Conditions on Condensation Heat Transfer in Rotating Heat Pipes", International Journal of Heat and Mass Transfer, Vol. 22, pp. 1237-1241.

Daniels,T.C. and Al-Jumaily, F.K., 1975, "Investigations of the Factors Affecting the Performance of a Rotating Heat Pipe", International Journal of Heat and Mass Transfer, Vol. 18, pp. 961-973.

Faghri, A., Gogineni, S. and Thomas, S., 1993, "Vapor Flow Analysis of an Axially Rotating Heat Pipe", International Journal of Heat and Mass Transfer, Vol. 36, No. 9, pp. 2293-2303.

Gray,V.H., 1969, "The Rotating Heat Pipe; a Wickless, Hollow Shaft for Transferring High Heat Fluxes", Proceedings of the ASME/AIChE Heat Transfer Conference, Minneapolis, USA, pp.1-5.

Harley, C. and Faghri, A., 1995, "Two-dimensional Rotating Heat Pipe Analysis", Journal of Heat Transfer-Transactions of the ASME, Vol. 117, pp. 202-208.

Ismail, K.A.R. and Miranda, R.F., 1997, "Two-dimensional Axisymmetrical Model for a Rotating Porous Wicked Heat Pipe", Applied Thermal Engineering, Vol. 17, No. 2, pp. 135-155.

Li, H.M., Liu, C.Y. and Damodaran, M., 1993, "Analytical Study of the Flow and Heat Transfer in a Rotating Heat Pipe", Heat Recovery Systems & CHP Vol. 13, No.2, pp. 115-122.

Miranda, R. F., 1989, "Desenvolvimento de um Modelo Matemático para a Análise Local do Desempenho de Tubos de Calor, com Rotação em seu Eixo Axial", Ph.D. thesis, University of Campinas, Brazil.

Patankar, S.V., 1980, "Numerical Heat Transfer and Fluid Flow", Hemisphere Publishing Corporation, U.S.A., 197 p.

Ponnappan, R. and He, Q., 1998, "Test Results of Water and Methanol High-Speed Rotating Heat Pipes", Journal of Thermophysics and Heat Transfer, Vol. 12, pp. 391-397.

Saraiva, L. E., 2004, "Simulação Numérica para Análise Local e Global do Desempenho de Tubos de Calor Rotativos com Estrutura Porosa", PhD thesis, University of Campinas, Brazil.

Saraiva, L.E. and Ismail, K.A.R., 2006, "A Numerical Parametric Study of a Cylindrical Non-tapered Axially Rotating Porous Heat Pipe (submitted for publication)